Experimental evidence for the survival of augite to transition zone depths, and implications for subduction zone dynamics

JINGUI XU[1,2,3], DONGZHOU ZHANG[2], PRZEMYSLAW DERA[2], BO ZHANG[1,3], AND DAWEI FAN[1,*]

[1]Key Laboratory of High Temperature and High Pressure Study of the Earth's Interior, Institute of Geochemistry, Chinese Academy of Sciences, Guiyang, 550081, China
[2]Hawaii Institute of Geophysics and Planetology, School of Ocean and Earth Science and Technology, University of Hawaii at Manoa, 1680 East West Road, POST Building, Honolulu, Hawaii 96822, U.S.A.
[3]University of Chinese Academy of Sciences, Beijing, 100049, China

ABSTRACT

(Ca,Mg)-rich clinopyroxenes are abundant in Earth's upper mantle and subduction zones. Experimental studies on the thermoelastic properties of these minerals at simultaneous high pressure and high temperature are important for constraining of the composition and structure of the Earth. Here, we present a synchrotron-based single-crystal X-ray diffraction study of natural diopside-dominated augite [$(Ca_{0.89}Na_{0.05}Mg_{0.06})(Mg_{0.74}Fe_{0.11}Al_{0.14}Ti_{0.01})(Si_{1.88}Al_{0.12})O_{6.00}$] at P and T to ~27 GPa and 700 K. The experiment simulates conditions in cold subducting slabs, and results indicate that augite is stable over this pressure and temperature range. A third-order high-temperature Birch-Murnaghan equation was fit with the pressure-volume-temperature data, yielding the following thermoelastic parameters: K_{T0} = 111(1) GPa, K'_{T0} = 4.1(1), $(\partial K_0/\partial T)_P$ = –0.008(5) GPa/K and α_T = 4(1)×10^{-5} K^{-1} +2(3)×10^{-8} K^{-2} T. A strain analysis shows that the compression along the three principal stress directions is highly anisotropic with ε1:ε2:ε3 = 1.98:2.43:1.00. Additionally, high-pressure structural refinements of room-temperature polyhedral geometry, bond lengths and O3-O3-O3 angle were investigated to ~27 GPa at ambient temperature. Pressure dependences of polyhedral volumes and distortion indicate that the substitution of Al^{3+} for Si^{4+} significantly changes the compressional behavior of the TO_4-tetrahedron in augite. Density calculations of this augite along a subducting slab geotherm suggest that augite as well as other common clinopyroxenes would promote slab stagnations at transition zone depths if they are metastably preserved in significant quantities.

Keywords: Pyroxenes, augite, high pressure and temperature, single-crystal X-ray diffraction, subduction zone

INTRODUCTION

Pyroxenes are among the most important rock-forming minerals and are commonly found in both igneous and metamorphic rocks. Oceanic lithosphere consists of about 40% pyroxenes and garnet (Frost 2008). It was believed that pyroxenes transform into denser majorite garnet while oceanic crust subducts into the mantle (Akaogi and Akimoto 1977). However, recent studies imply that this reaction is inhibited under cold slab conditions, so pyroxenes may survive in deeper parts of the mantle than was previously thought (Nishi et al. 2008, 2013; Van Mierlo et al. 2013). Surviving metastable pyroxenes might cause stagnations of some slabs at depths along the 660 km discontinuity, due to their lower densities compared to garnet and broader metastability range compared to the metastable olivine (Agrusta et al. 2014; King et al. 2015; Nishi et al. 2013; Van Mierlo et al. 2013). Therefore, knowledge of the properties of pyroxenes to transition zone pressures (≥25 GPa) is very important in modeling the subduction zone environments.

Among the pyroxene group minerals, augite is the most

common species and occurs in basalts and gabbros, which are major components of the oceanic crust. Augite is also commonly found in andesites, diorites, peridotites, and pyroxenites. Augite is monoclinic (*C2/c* space group) and has relatively complex crystal chemistry. Pyroxenes have a general formula of $M2M1T_2O_6$. In augite, *M*1 sites are usually filled with Mg^{2+}, Fe^{2+}, Ti^{3+}, and Al^{3+}; *M*2 are larger polyhedral sites that commonly accommodate Ca^{2+}, Na^+, Fe^{2+}, and Mg^{2+}; while *T* sites are occupied predominantly by Si^{4+}, but typically contains some Al^{3+} (Clark et al. 1969). In contrast with augite, diopside [$CaMgSi_2O_6$] and hedenbergite [$CaFeSi_2O_6$] are usually Al free. Although pyroxene minerals have been extensively investigated at high pressures with the discovery of several new polymorphs (Dera et al. 2013a; Finkelstein et al. 2014; Plonka et al. 2012; Zhang et al. 2012), studies of augite at high pressures and temperatures have been limited. Augite is important to the petrology of subducted slabs, therefore it seems urgent to fill the gap in understanding of the compressional behavior of this mineral at simultaneous high pressures and temperatures. In this study, single-crystal X-ray diffraction measurements of natural augite were conducted at 0–26.65(2) GPa at ambient temperature and the crystal structures were refined. The *P-V-T*

relations were measured at pressure-temperature conditions to 24.35(2) GPa and 700 K, and thermal equation of state was determined. We discussed the potential effect of metastable augite on subducting slab dynamics in this report.

SAMPLES AND METHODS

Natural augite samples were collected from the Damaping pyroxenite, Zhangjiakou, Hebei Province, China. The crystals were colored light green, and their chemical was estimated as $[(Ca_{0.89}Na_{0.05}Mg_{0.06})(Mg_{0.74}Fe_{0.11}Al_{0.14}Ti_{0.01})(Si_{1.88}Al_{0.12})O_{6.00}]$ based on results of electron microprobe analysis (EMPA). Small chips (size 0.035×0.040 mm) of single-crystal augite with thicknesses less than 0.010 mm were extracted from a larger EMPA sample for this study. A single crystal was first mounted onto a polymer micromesh sample holder (MiTeGen) for ambient-condition X-ray diffraction study. One single crystal was used for each high pressure/temperature experiment. A BX90 DAC (Kantor et al. 2012) was used for high-pressure measurements at ambient temperature. This DAC was equipped with two type-I diamond (300 μm culets) mounted on Boehler-Almax-type WC seats, which had ±30° opening angles. A rhenium gasket was used and pre-indented to ~40 μm thickness before a laser drilling of a 190 μm diameter hole. The augite sample was loaded into the sample chamber with Au powder serving as the pressure calibrant (Fei et al. 2007). At each pressure, Au diffraction patterns were collected before and after sample data collection and the average pressure values were used. A small ruby sphere of ~10 μm was also loaded and used as the pressure indicator for the gas-loading with Ne as the pressure-transmitting medium using the GSECARS gas-loading system (Rivers et al. 2008). An externally heated DAC (EHDAC) was used for high-pressure and high-temperature experiments. Temperatures up to 700 K were generated by resistive-heating and measured with a K-type thermocouple attached to one of the anvils ~500 μm away from the diamond culet. Likewise, Au powder, a ruby sphere and a single-crystal sample were loaded, and Ne was used for pressure-transmitting medium.

All of the X-ray diffraction experiments in this study were carried out at experimental station 13-BM-C of the Advanced Photon Source, Argonne National Laboratory. The incident X-ray beam was monochromated to a wavelength of 0.4340 Å, and collimated to a focal spot size of 15×15 μm². Diffraction images were acquired on a MAR165 CCD detector (Zhang et al. 2017). Tilting and rotation of the detector and the sample-to-detector distance were calibrated using ambient LaB₆ as the diffraction standard. To obtain adequate number of diffraction for structure refinements, we collected data at 4 different detector positions achieved by rotating the detector on the 6-circle goniometer. At D1 position the detector was perpendicular to the incident X-ray direction, D2 was achieved by rotating the detector about the horizontal axis by 20°, whereas D3 and D4 were involved rotating about the vertical axis by 10° and –10°, respectively. Wide and stepped φ exposures were collected for single-crystal samples at each P-T point at D1 position, with an exposure time of 2 s/°. Wide segment exposures with 10° rotation step were collected at each detector position. The φ scan rotation axis was horizontal and perpendicular to the incident X-ray direction.

The ATREX/RSV software package (earlier known as GSE_ADA/RSV, Dera et al. 2013b), was used to analyze the diffraction images. The lattice parameters and orientation matrix were determined with the RSV software and the reduced reflection data from the four detector positions were merged together. Unit-cell parameters at each P-T condition are reported in Table[1] 1. Crystal structures of augite at high pressures were refined from the intensity data using SHELXL software via the Olex 2 user interface (Dolomanov et al. 2009; Sheldrick 2007), starting from atomic coordinates of Clark et al. (1969). According to the microprobe chemistry and previously reported augite structure model (Clark et al. 1969), the site occupancies were refined without vacancies. The M2 sites were fully occupied by Ca^{2+}, Mg^{2+}, and Na^+; Fe^{2+}, Mg^{2+}, Ti^{3+}, and Al^{3+} occupied the M1 sites, while the T sites contained Si^{4+} and Al^{3+}. Cations in the same polyhedral site were set to share the same atomic displacement parameters (ADPs) and the same fractional coordinates. The anisotropic ADPs were only used for cations, due to the limited number of unique observations. At ambient pressure the site-occupancy refinement for the M2, M1, and T sites led to a mean electron number of 19.2, 13.4, and 14.0, which are very close to the numbers calculated on the basis of

the chemical data (19.1, 13.8, and 13.9 for M2, M1, and T sites, respectively). The refined sum of mean electron number is also in general agreement with the microprobe composition, so the cation contents based on the EMPA composition were used in refinements. We also modeled the site distribution of Fe between M2 and M1 sites, and the result indicated that the M2 site is free of Fe. Previous studies suggested that Fe^{3+} could be included in M1 sites in addition to Fe^{2+}, based on Mössbauer measurements and other calculation methods, but only in small quantities (Clark et al. 1969). Clark et al. (1969) proposed a method to infer the Fe^{3+}/Fe^{2+} distribution in augite based on the M1-O distance values. In this approach M1-O distance in augite is assumed to be a simple linear combination of the average M1-O distances observed in various end-member compositions. According to this method and the use of the M1-O values of jadeite $[NaAlSi_2O_6]$, diopside $[CaMgSi_2O_6]$, aegirine $[NaFeSi_2O_6]$ (Clark et al. 1969), hedenbergite $[CaFeSi_2O_6]$ (Zhang et al. 1997), and $[NaTiSi_2O_6]$ (Ullrich et al. 2010) combined with the M1-O value in this study, we concluded that our augite sample is free of Fe^{3+}. In high-pressure refinements the site occupancy parameters of the cations were fixed based on the EMPA and ambient-pressure structure refinement. Details of the structural refinements, atomic coordinates, bond lengths and angles are reported in Tables[1] 2, 3, and 4. Because of the limited opening angle (±17°) of the EHDAC, the structure refinements were not possible.

RESULTS AND DISCUSSION

Equation of state of augite at 298 K

Figures 1 and 2 present the unit-cell parameters of augite as a function of pressure. V, a, b, c, and β angle undergo nonlinear decrease to 26.65(2) GPa with no discontinuity in the compression curves. A third-order Birch-Murnaghan equation of state (BM3 EoS) was fit with the P-V data using the EosFit7c program (Angel et al. 2014). The isothermal bulk modulus (K_{T0}) and its pressure derivative (K'_{T0}) were calculated to be 111(1) GPa and 4.1(2). The Eulerian finite strain ($f_E = [(V_0/V)^{2/3} - 1]/2$) vs. "normalized pressure" $\{F_E = P/[3f_E(2f_E + 1)^{5/2}]\}$ plot (Angel 2000) was also used to analyze the P-V data, and a weighted linear fit yielded an intercept value of 111(1) GPa, which is in good agreement with the results indicated by BM3 EoS (Fig. 3). The linear moduli of a, b, and c were also calculated using the linear BM3 equation (Fig. 1) and EosFit7c program. The compressibilities (β) (Angel 2000) of each axis were calculated (Table[1] 5) yielding $\beta_a:\beta_b:\beta_c = 1:1.44:1.11$, which shows that b has the highest compressibility and c is more compressible than a.
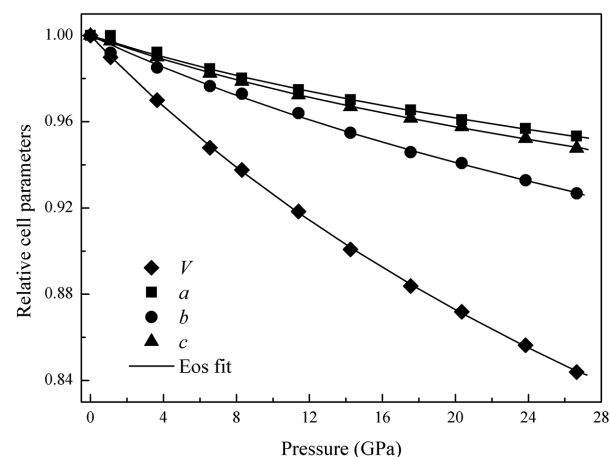
FIGURE 1. Normalized unit-cell volume and lattice parameters (a, b, and c) of augite as a function of pressure at room temperature. The error bars of the data points are smaller than the symbols.
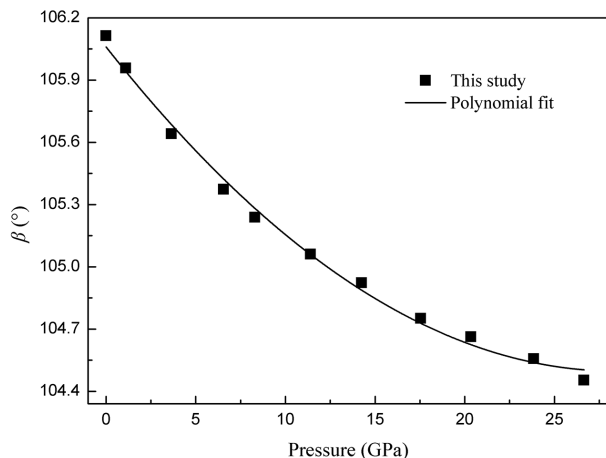
FIGURE 2. Pressure dependence of β angle at ambient temperature. The error bars of the data points are smaller than the symbols.

Strain analysis

Strain tensor analysis was performed to assess the degree of anisotropy between principal stress directions, because the *a*- and *c*-axis are not the principal strain axes while *b*-axis is coincident with one of them. Unit-cell parameters of augite were used to analyze unit strain ellipsoid with win_STRAIN (Angel 2015), modified after Ohashi (1982). Table[1] 6 shows the strain values and directions of the three major compression axes at each pressure. To visualize the orientation of the strain tensor, we calculated the representation quadratic surface of augite using the method suggested by Knight (2010). As shown in Figure 4, the softest major axis is parallel to the *b*-axis, and the stiffest direction is oriented in the *a-c* plane.

Polyhedral compression and distortion

The evolutions of the volume of the $M2O_8$-polyhedron, $M1O_6$-octahedron and TO_4-tetrahedron with increasing pressure were investigated and shown in Figures 5 and 6. The eightfold-coordinated $M2O_8$-polyhedron is the most compressible while
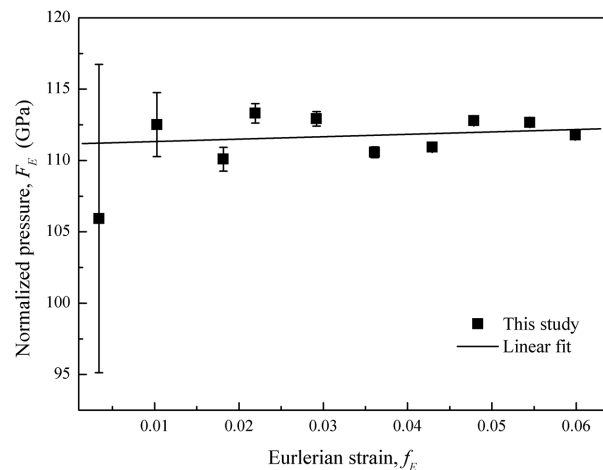
FIGURE 3. Eulerian strain-normalized pressure (F_E-f_E) plot of unit-cell volume.
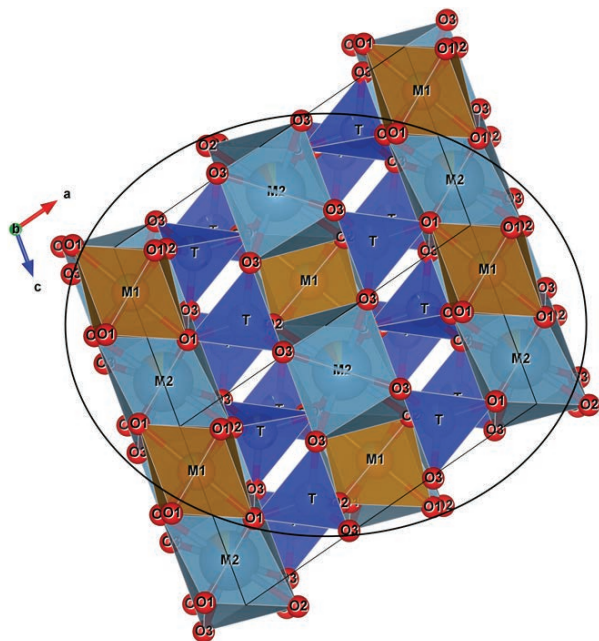
FIGURE 4. The orientation of the representation quadric for the isothermal compressibility tensor of augite at 26.65 GPa, viewed down *b*. (Color online.)
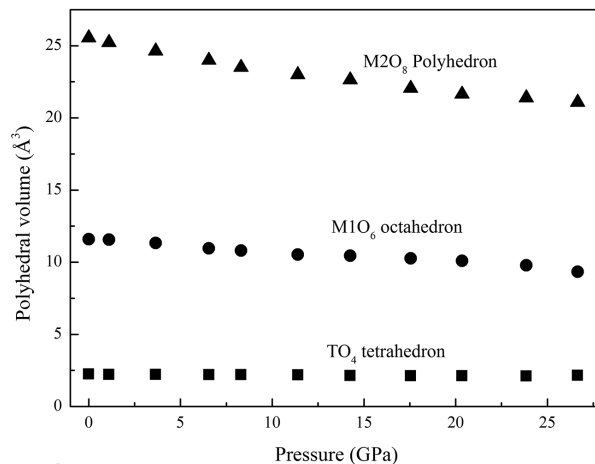
FIGURE 5. Pressure dependences of $M1O_6$, $M2O_8$, and TO_4 polyhedral volumes. The error bars of the data points are smaller than the symbols.

the TO_4-tetrahedron is the least. Likewise, the compression of the $M2O_8$-polyhedron is the smoothest, and the TO_4-tetrahedron is the least smooth. The distortions of these polyhedra were also analyzed (Robinson et al. 1971). As shown in Figure 7 the distortion index of the $M2O_8$-polyhedron decreases quickly with increasing pressure up to ~15 GPa, where it becomes less responsive to pressure. This change can be explained by examining evolutions of the bond lengths with pressure. As shown in Figure 8 the longest bonds $M2$-O3(C2, D2) becomes comparable to other bonds at about 15 GPa. The $M1O_6$-octahedron has the smallest distortion index, which decreases to the minimum at ~20 GPa, and then increases again to a value comparable to the ambient distortion (Figs. 7 and 9).
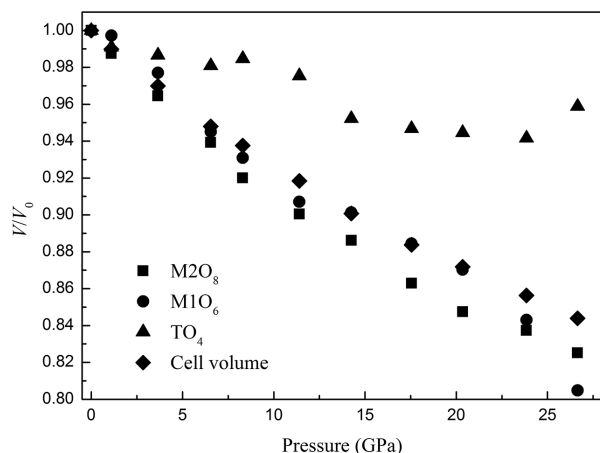
FIGURE 6. Pressure dependences of the polyhedral and unit-cell volumes. The error bars of the data points are smaller than the symbols.
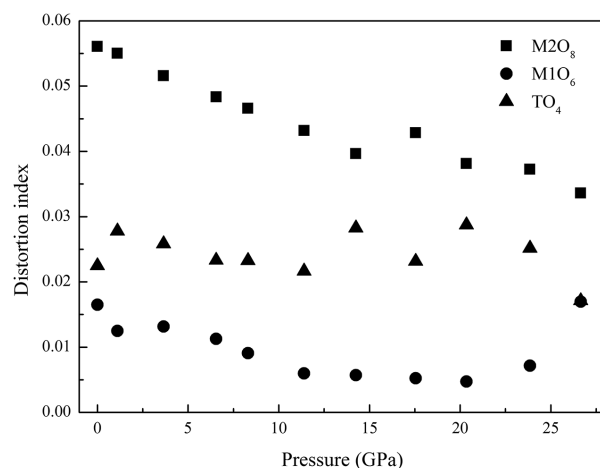
FIGURE 7. Pressure dependences of distortion indices of different polyhedral.

Thermal equation of state

The unit-cell parameters of augite at various P-T conditions are given in Table[1] 1, and were used for subsequent calculations. Figure 12 shows the volume data measured at 298, 500, and 700 K. The high-temperature Birch-Murnaghan (HTBM) equation was fit with the P-V-T data. The equation is given by the following form:

$$P = \tfrac{3}{2}K_{T0}\left[(V_{T0}/V)^{7/3} - (V_{T0}/V)^{5/3}\right] \times \left\{1 + \tfrac{3}{4}(K'_{T0}-4)[(V_{T0}/V)^{2/3}-1]\right\} \tag{1}$$

where K_{T0}, K'_{T0}, and V_{T0} are bulk modulus, its pressure derivative and the unit-cell volume at ambient pressure and temperature (in Kelvin), respectively. The effects of temperature on K_{T0} and V_{T0} are expressed by the follows:

$$V_{T0} = V_0 \exp\int_{300}^{T}\alpha_T dT \tag{2}$$
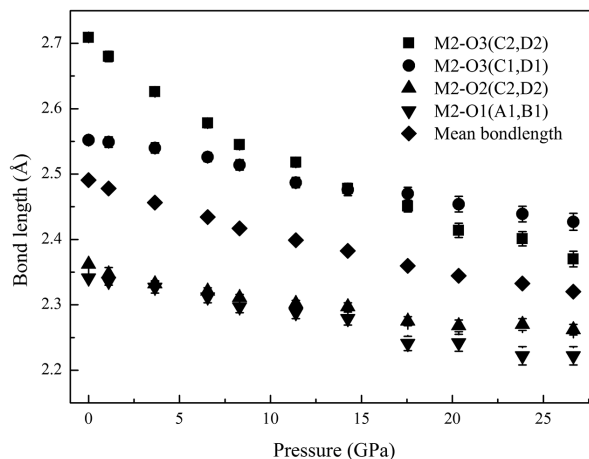
FIGURE 8. Pressure dependences of the M2-O bond lengths in $M2O_8$ polyhedron.
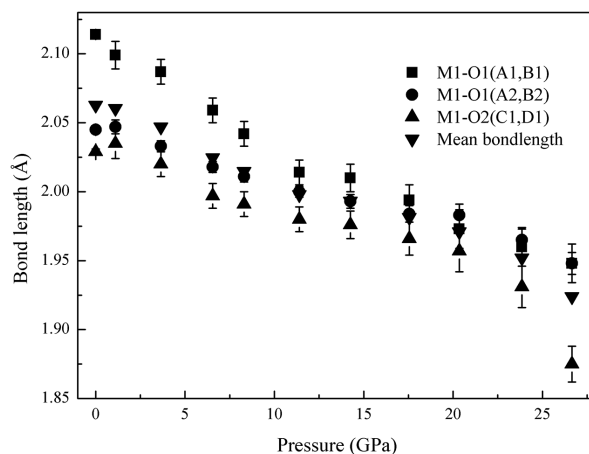
FIGURE 9. Pressure dependences of the M1-O bond lengths in $M1O_6$ polyhedron.

Pyroxenes are characterized by single chains of tetrahedra that extend parallel to the c-axis. These chains have significant rotation freedoms at high pressures, which can be described by the reduction of the O3-O3-O3 angle (Figs. 10 and 11). The ∠O3-O3-O3 of augite shows a linear decrease of approximately –0.47 °/GPa in the pressure range of 0–8.30(4) GPa, then experiences a minor increase with increasing pressure between 8.30(4) and 11.40(3) GPa (Table[1] 4 and Fig. 11). This is similar to what was reported for kosmochlor [NaCrSi$_2$O$_6$] (Posner et al. 2014), in which the inflection occurs at 31.3 GPa. In augite this "hardening" of rotation of tetrahedral chains is accompanied by a volume drop of TO_4-tetrahedra in augite (Fig. 6), which was also observed in kosmochlor (Posner et al. 2014). Above 11.40(3) GPa, the ∠O3-O3-O3 decreases again, this time at an approximate rate of (0.37 °/GPa), as the TO_4-tetrahedra become more incompressible (Fig. 6). However, the pressure-dependencies of the unit-cell volume and lattice parameters do not exhibit any distinct discontinuities correlated with this curious behavior of the O3-O3-O3 angle (Figs. 1 and 2).

$$K_{T0} = K_0 + (\partial K_0/\partial T)_P \times (T - 298) \qquad (3)$$

$$\alpha_T = \alpha_0 + \alpha_1 T \qquad (4)$$

where $(\partial K_0/\partial_T)_P$ and α_T are the temperature derivative of the bulk modulus and the volumetric thermal expansion at ambient pressure.

Fitting the P-V-T data to the HTBM (1) yielded $K_{T0} = 111(1)$ GPa, $K'_{T0} = 4.1(1)$, $(\partial K_0/\partial T)_P = -0.008(5)$ GPa/K and α_T (K^{-1}) = $4(1) \times 10^{-5} + 2(3) \times 10^{-8}$ T. In view of the relatively low-temperature range (298–700 K in this study) and limited high-temperature data, α_T is often assumed to be constant over the temperature range i.e., $\alpha_T = \alpha_0$ (e.g., Nishihara et al. 2003; Xu et al. 2016). Therefore, the P-V-T data were also fitted by constraining $\alpha_T = \alpha_0$, which yielded $K_{T0} = 111(1)$ GPa, $K'_{T0} = 4.1(1)$, $(\partial K_0/\partial T)_P = -0.008(5)$ GPa/K and α_T (K^{-1}) = $5.1(3) \times 10^{-5}$. The K_{T0} values derived from high-temperature and -pressure data are in excellent agreement with that from EoS fit at ambient temperature [$K_{T0} = 111(1)$ GPa].

FIGURE 12. The unit-cell volume as a function of pressure and temperature.
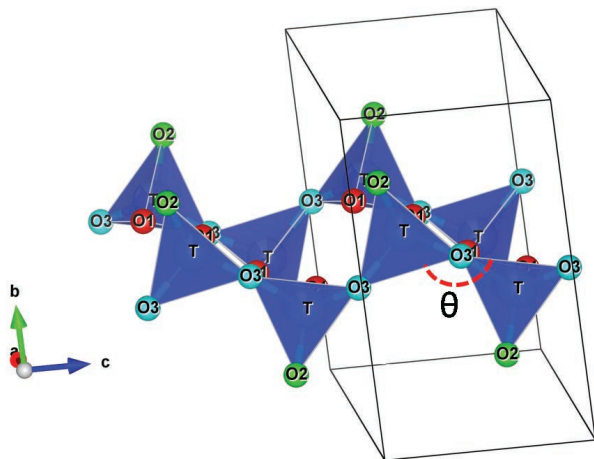
FIGURE 10. An illustration of the O3-O3-O3 angle. (Color online.)
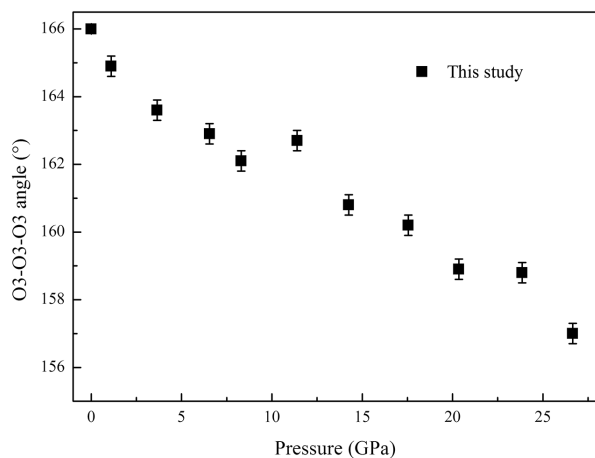
FIGURE 11. Tetrahedral chains kinking as described by O3-O3-O3 angle as a function of pressure.

Comparison with previous studies

Due to the compositional complexity of augite, it is necessary to evaluate the effects of cation substitutions on polyhedral compressions. Here we compared the polyhedral compressions of augite and other important clinopyroxene end-members including jadeite [NaAlSi$_2$O$_6$], diopside [CaMgSi$_2$O$_6$], hedenbergite [CaFe^{2+}Si$_2$O$_6$], and aegirine [NaFe^{3+}Si$_2$O$_6$], all of which have $C2/c$ symmetry. In these pyroxenes the $M2$ site is normally occupied by Ca^{2+} (eightfold-coordinated) and Na$^+$ (sixfold-coordinated) (Downs 2003), and the Ca^{2+}- and Na$^+$-polyhedra exhibit about comparable compression below ~8 GPa, above which the Ca^{2+}-polyhedra are more incompressible than Na-polyhedra. Our augite has minor Na and Mg contents in addition to Ca^{2+} occupying the $M2$ site, but this substitution does not distinctly change the compression behavior of the Ca^{2+}-dominated polyhedral, as shown in Figure 13a. In comparison with the $M2$ site, different cations occupying the $M1$ site have distinct effects on the compression of the $M1$-octahedron (Fig. 13b). The $M1$ site fully occupied by Al^{3+} is the most incompressible among these clinopyroxenes, while the Mg-octahedron is the most compressible. Fe^{2+}- and Fe^{3+}-octahedra have distinctly different compression trends, with the latter being stiffer (McCarthy et al. 2008b), and comparable to the Al^{3+}-octahedron, while Fe^{2+}-octahedron is nearer to the Mg^{2+}-octahedron. The $M1$ site of augite in this study is mainly Mg^{2+}-occupied, but has significant contents of Fe^{2+} and Al^{3+}, and below ~11 GPa the compression of the octahedron is similar to that of Mg^{2+}-octahedron in diopside. Above ~11 GPa, it becomes stiffer and closer to the trend of the Fe^{2+}-octahedron in hedenbergite. The T site is almost fully filled by Si^{4+} in most pyroxene minerals, but can contain small amount of Al^{3+} in augite (e.g., Bindi et al. 2003; Hazen and Finger 1977). In this study we investigated the effect of the incorporation of Al^{3+} into the T site on the tetrahedral compression. As shown in Figure 13c, the Al-free end-member $C2/c$ pyroxenes display very similar tetrahedral compression trends, while the compression of the T-tetrahedron augite is notably different, below ~13 GPa it also results in the compression trend, however, after that it has a distinct volume drop at ~14 GPa as indicated by the pressure dependences of the
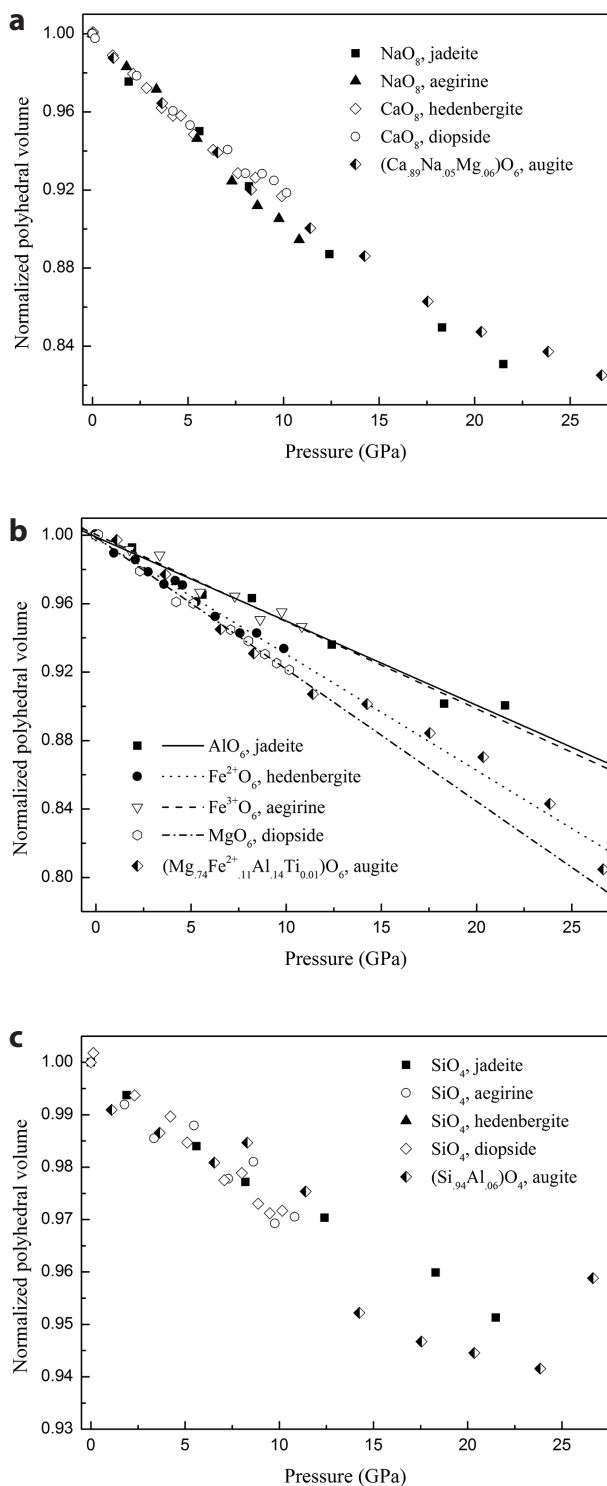
FIGURE 13. Polyhedral volumes as a function of pressure in jadeite (Posner et al. 2014), aegirine (McCarthy et al. 2008b), hedenbergite (Zhang et al. 1997), diopside (Thompson and Downs 2008) and augite (this study). Panels **a**, **b**, and **c** are $M2$-polyhedron, $M1$-octahedron, and T-tetrahedron, respectively.

O3-O3-O3 angle and the T-O bond lengths (Figs. 11 and 14). We also used a second-order BM EOS to calculate the zero-pressure bulk modulus (K_{T0}) values of these T-tetrahedra, and the results suggest that augite has a larger tetrahedral K_{T0} [345(30) GPa] than aegirine [328(22) GPa], hedenbergite [306(16) GPa], and diopside [321(15) GPa], but smaller than jadeite [386(10) GPa]. Therefore, the tetrahedral K_{T0} values of clinopyroxenes depend not only on cations occupying the T sites. To summarize, the incorporation of Na^+ and Mg^{2+} does not significantly change the $M2$-polyhedral compression in augite. The substitutions of Fe^{2+} and Al^{3+} in the $M1$ site, however, cause a distinct $M1$-octahedral compression change after ~11 GPa. The most significant effect of the cation substitution occurs in the T site, with an evident tetrahedral volume drop during the compression.

The K_{T0} value of augite (whole crystal) obtained in this work was also compared with previous investigations of jadeite, diopside, hedenbergite, and aegirine. It is clear that the polyhedral compression is not the only factor that constrains the K_{T0} values of these pyroxenes. Among these $C2/c$ pyroxenes jadeite has the most incompressible $M1$-octahedron and the largest K_{T0} value that ranges from 124.5(4) to 136.5(14) GPa (McCarthy et al. 2008a; Nestola et al. 2006; Posner et al. 2014; Zhao et al. 1997), and hedenbergite [$CaFe^{2+}Si_2O_6$] and aegirine [$NaFe^{3+}Si_2O_6$] have nearly identical K_{T0} values [116.1(5)–117(1) GPa] (Downs and Singh 2006; McCarthy et al. 2008b; Nestola et al. 2006; Zhang et al. 1997; Zhao et al. 1998), even though the Fe^{2+}-octahedron is much more compressible than the Fe^{3+}-octahedron. Previous studies on diopside give a relatively large range of K_{T0} values [104.1(9)–118(1) GPa] (Aleksandrov and Rythova 1961; Levien and Prewitt 1981; Thompson and Downs 2008; Zhang et al. 1997). In this study, the K_{T0} value [111(1) GPa] of a diopside-dominant augite derived from a BM3 Eos fitting of the P-V data are also within the value range of the pure diopside, although significant Al^{3+} and Fe^{2+} were incorporated in the $M1$ and T sites.

Numerous thermal expansion studies have been conducted on pyroxene minerals, and the values of α_T show a large variation range (1.84–9.26×10^{-5} K^{-1}) with various compositions and structures (see summarizations in Yang and Prewitt 2000
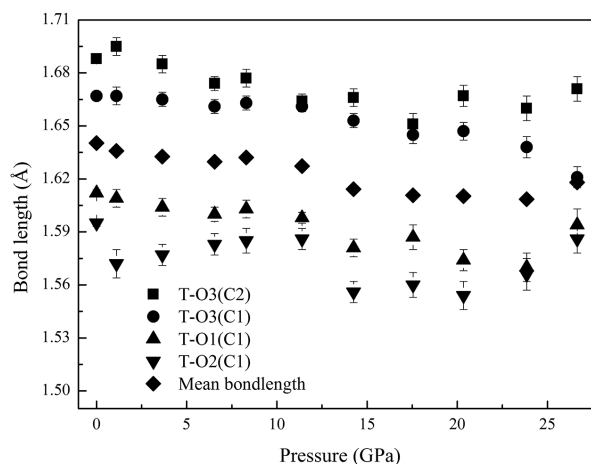
FIGURE 14. Pressure dependences of the T-O bond lengths in TO_4 polyhedron.

and Tribaudino and Mantovani 2014). Augite in this study is diopside-rich and has a α_T value of $5.1(3) \times 10^{-5}$ K^{-1}, which is higher than that of previous studies of diopside end-member [$CaMgSi_2O_6$] ($3.41–3.44 \times 10^{-5}$ K^{-1}) (Finger and Ohashi 1976; Richet et al. 1998). The discrepancy is likely due to the compositional difference. Augite in this study has significant contents of Al in the $M1$ and T sites, compared to the end-member-diopside. Incorporation of Al was previously regarded as a reason for decrease in the thermal expansion (Tribaudino and Mantovani 2014).

IMPLICATIONS

Clinopyroxenes are major components of Earth's upper mantle. The (Ca,Mg)-rich clinopyroxenes provide important constraints when modeling the mineralogy of the upper mantle (Frost 2008). At normal mantle temperature condition clinopyroxes would disappear at transition zone depth because they are dissolved into majorite garnet (Ringwood 1982). However, clinopyroxenes could survive in subducting slabs to greater depths because the pyroxene-garnet transition would be inhibited at relatively low slab temperatures (Bina 2013; Nishi et al. 2013; Van Mierlo et al. 2013). On the other hand, high-pressure experimental studies demonstrate that common Ca- and Na-rich clinopyroxenes (with $C2/c$ space group) like diopside [$CaMgSi_2O_6$], hedenbergite [$CaFeSi_2O_6$] and jadeite [$NaAlSi_2O_6$] are stable even at very high pressures. Diopside retains its $C2/c$ symmetry to ~50 GPa at room temperature and transforms to the β-$CaMgSi_2O_6$ phase at ~56 GPa (Chopelas and Serghiou 2002; Plonka et al. 2012). High-pressure diffraction and Mössbauer studies of hedenbergite also show that it is stable over 50 GPa until two discontinuities take place at 53 and 68 GPa (Hu et al. 2015; Zhang et al. 1999). Jadeite is also stable at high pressures to 30 GPa (Posner et al. 2014), and the jadeite-diopside solid solution has no phase transition within pressure range of 0–47 GPa (Zhang et al. 2016). Aegirine [$NaFe^{3+}Si_2O_6$] also retains its symmetry to ~60 GPa, even though a Na-coordination change induced isosymmetric phase transition takes place at ~24 GPa (Xu et al. 2017). Based on these studies one can expect that Ca- and Na-rich clinopyroxenes within the CaO-Na_2O-MgO-$Fe^{(2+/3+)}$O-Al_2O_3-SiO_2 system, which are important to the upper mantle and subduction zones, have large pressure ranges of metastabilities (possibly 0–50 GPa at ambient temperature), however extensive studies of the temperature effects are required (e.g., Nishihara et al. 2003; Zhao et al. 1998, 1997). Among the $C2/c$ clinopyroxenes augite is the most common and occurs in various igneous rocks like basalt, gabbro, and peridotite, and also in metamorphic rocks like gneiss, schist, and granulite (Banno 1959; O'Har 1961; Otten and Buseck 1987; Rooney et al. 2005; Schlinger and Veblen 1989; Schorn and Diener 2016; Takeda et al. 1997; Tracy and Robinson 1977). In this study the diopside-rich augite was found to be metastable at simultaneously high pressure and temperature to ~27 GPa and 700 K. Recently, the topic of metastable preservation of pyroxenes to significant depths in cold slabs has attracted increasing attention, and is treated as one of the explanations of the stagnations of some subducting slabs near the base of the mantle transition zone (Agrusta et al. 2014; Bina 2013; King et al. 2015; Nishi et al. 2013; Van Mierlo et al. 2013). The main reason is that pyroxene

is the least dense mineral in the pyrolitic assemblage, and the density difference between the slabs and surrounding mantle is a key factor that controls buoyancy, however, other factors like viscosity also need to be considered (Agrusta et al. 2014; Nishi et al. 2013). Pyroxenes can survive even at high temperatures, while in contrast, metastable olivine can only persist under very cold conditions (Nishi et al. 2008, 2009). Even so, deciphering the effects of metastable pyroxenes on slab dynamics still requires a lot of further measurements, including density and elasticity of relevant minerals at simultaneous high-pressure and temperature conditions. However, such work on pyroxenes is limited (e.g., Akashi et al. 2009; Nishihara et al. 2003; Zhao et al. 1998, 1997), and the pressure range is relatively low compared to transition zone depth. In this study we conducted single-crystal X-ray diffraction measurements on natural augite at simultaneously high-pressure and temperature to ~27 GPa and 700 K, simulating conditions within the coldest part of a subducting slab. The diffraction data reveal that augite is metastable within this range of P-T condition, and the P-V-T data were used to calculate related thermoelastic parameters.

To date, numerous seismic studies on subducting slab morphology show that most slabs are denser than the mantle before they sink into the transition zone depths, where the densities of slabs and surrounding mantle become comparable (Fig. 15). However, depending on the slab geometry and thermal structure become different, some subducted slabs sink into the lower mantle (e.g., Center America), while others stagnate (e.g., Tonga) (Fukao and Obayashi 2013; Fukao et al. 2001; Grand 2002; Kawakatsu and Yoshioka 2011; Li et al. 2008; Van der Hilst et al. 1997). Density is the principle factor controlling buoyancy, and the metastable pyroxene is a candidate contributor for slab stagnations (Agrusta et al. 2014; Bina 2013; King et al. 2015; Nishi et al. 2013; Van Mierlo et al. 2013). To better understand the effect of metastable pyroxenes on the slab dynamics we calculated the density profiles of augite and other common mantle pyroxene minerals along a geotherm that is typical for cold subduction (Ganguly et al. 2009). The third-order HTBM equation (formula
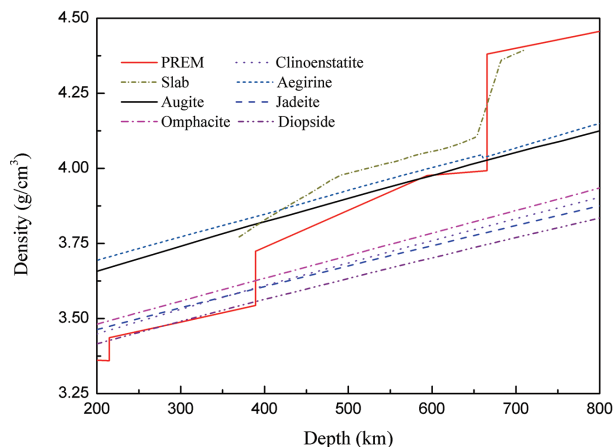
FIGURE 15. Calculated density profiles of augite as well as other common clinopyroxenes to ~800 km, and the PREM (Dziewonski and Anderson 1981) model and the density profile of a Tonga-type slab (Ganguly et al. 2009) are also showed. (Color online.)

TABLE 7. Thermoelastic properties of high pressure minerals used for density calculations

Mineral	V_0 (Å³)	K_{T0} (GPa)	K'_{T0}	$\partial K_0/\partial_T$	$a_0 \times 10^{-5}$	$a_1 \times 10^{-8}$ (K⁻¹)
Jadeite[a]	403.32(8)	124.5(4.0)	5.0(fixed)	−0.016(5)	2.56(22)	0.26(18)
Aegirine[b]	431.5(1)	118(3)	4.2(3)	−0.016(5)	2.64(13)	0
Diopside[c]	438.67(6)	109(4)	4.8(6)	−0.021(4)	2.32(5)	1.88(7)
Omphacite[d]	424.7(7)	126(1)	4.0(fixed)	−0.015(4)	2.2(1)	0
Clinoenstatite[e]	405.0(2.6)	106.9(25.9)	5.3(3.9)	−0.021(10)	2.01(44)	2.1(1.1)

Notes: References: [a] Zhao et al. (1997); [b] Tribaudino et al. (2008) and Xu et al. (2017), note that $\partial K_0/\partial T$ was assumed to be the same as in jadeite (no data of $\partial K_0/\partial T$ for aegirine is currently available); [c] Zhao et al. (1998); [d] Nishihara et al. (2003); [e] Shinmei et al. (1999).

1–4) was used, and the minerals and related themoelastic parameters are shown in Table 7. The results comparing the PREM model (Dziewonski and Anderson 1981) and a Tonga-type slab (Ganguly et al. 2009) are presented in Figure 15. In this figure augite $[(Ca_{0.89}Na_{0.05}Mg_{0.06})(Mg_{0.74}Fe_{0.11}Al_{0.14}Ti_{0.01})(Si_{1.88}Al_{0.12})O_{6.00}]$ and aegirine $[NaFe^{3+}Si_2O_6]$ are notably denser than other pyroxenes (jadeite $[NaAlSi_2O_6]$, diopside $[CaMgSi_2O_6]$, omphacite $[Di_{63}Jd_{37}]$, and clinoenstatite $[Mg_2Si_2O_6]$) because of their higher Fe contents. At depth above the transition zone these Fe-free pyroxenes have densities closer to PREM pyrolite, while in the transition zone densities of augite and aegirine are more comparable to the PREM. On the other hand, the Tonga-type slab is significantly denser than all of these pyroxenes at depth below ~425 km. One could conclude that the presence of the Fe-rich pyroxenes like augite and aegirine would promote the sinking of slabs into the transition zone at the 410 km discontinuity. At the 660 km boundary as the ringwoodite decomposes into much denser Mg-perovskite and ferropericlase (Green and Ringwood 1967; Ito and Takahashi 1989; Liu 1976), the slab and surrounding mantle densities become comparable, based on our calculations all of these pyroxenes would contribute to the stagnation of the slab if they are preserved in significant quantities.

REFERENCES CITED

Agrusta, R., Hunen, J., and Goes, S. (2014) The effect of metastable pyroxene on the slab dynamics. Geophysical Research Letters, 41(24), 8800–8808.
Akaogi, M., and Akimoto, S.-i. (1977) Pyroxene-garnet solid-solution equilibria in the systems $Mg_4Si_4O_{12}$-$Mg_3Al_2Si_3O_{12}$ and $Fe_4Si_4O_{12}$-$Fe_3Al_2Si_3O_{12}$ at high pressures and temperatures. Physics of the Earth and Planetary Interiors, 15(1), 90–106.
Akashi, A., Nishihara, Y., Takahashi, E., Nakajima, Y., Tange, Y., and Funakoshi, K.i. (2009) Orthoenstatite/clinoenstatite phase transformation in $MgSiO_3$ at high-pressure and high-temperature determined by in situ X-ray diffraction: Implications for nature of the X discontinuity. Journal of Geophysical Research, 114, B04206.
Aleksandrov, K., and Rythova, T. (1961) The elastic properties of rock forming minerals, pyroxenes and amphiboles. Bulletin of Academy of Sciences, USSR, Geophysical Series, 871–875.
Angel, R.J. (2000) Equations of state. Reviews in Mineralogy and Geochemistry, 41(1), 35–59.
——— (2015) Win_Strain Program for Strain Calculations, http://www.rossangel.net.
Angel, R.J., Gonzalez-Platas, J., and Alvaro, M. (2014) EosFit7c and a Fortran module (library) for equation of state calculations. Zeitschrift für Kristallographie, 229(5), 405–419.
Banno, S. (1959) Aegirinaugites from crystalline schists in Sikoku. Journal of Geological Society of Japan, 65, 652–657.
Bina, C.R. (2013) Mineralogy: Garnet goes hungry. Nature Geoscience, 6(5), 335–336.
Bindi, L., Safonov, O.G., Yapaskurt, V.O., Perchuk, L.L., and Menchetti, S. (2003) Letter. Ultrapotassic clinopyroxene from the Kumdy-Kol microdiamond mine, Kokchetav Complex, Kazakhstan: Occurrence, composition and crystal-chemical characterization. American Mineralogist, 88, 464–468.
Chopelas, A., and Serghiou, G. (2002) Spectroscopic evidence for pressure-induced phase transitions in diopside. Physics and Chemistry of Minerals, 29(6), 403–408.
Clark, J.R., Appleman, D.E., and Papike, J. (1969) Crystal-chemical characterization of clinopyroxenes based on eight new structure refinements. Mineralogical Society of America Special Paper, 2, 31–50.
Dera, P., Finkelstein, G.J., Duffy, T.S., Downs, R.T., Meng, Y., Prakapenka, V., and Tkachev, S. (2013a) Metastable high-pressure transformations of ortho-ferrosilite Fs 82. Physics of the Earth and Planetary Interiors, 221, 15–21.
Dera, P., Zhuravlev, K., Prakapenka, V., Rivers, M.L., Finkelstein, G.J., Grubor-Urosevic, O., Tschauner, O., Clark, S.M., and Downs, R.T. (2013b) High pressure single-crystal micro X-ray diffraction analysis with GSE_ADA/RSV software. High Pressure Research, 33(3), 466–484.
Dolomanov, O.V., Bourhis, L.J., Gildea, R.J., Howard, J.A., and Puschmann, H. (2009) OLEX2: a complete structure solution, refinement and analysis program. Journal of Applied Crystallography, 42(2), 339–341.
Downs, R.T. (2003) Topology of the pyroxenes as a function of temperature, pressure, and composition as determined from the procrystal electron density. American Mineralogist, 88(4), 556–566.
Downs, R.T., and Singh, A.K. (2006) Analysis of deviatoric stress from nonhydrostatic pressure on a single crystal in a diamond anvil cell: The case of monoclinic aegirine, $NaFeSi_2O_6$. Journal of Physics and Chemistry of Solids, 67(9-10), 1995–2000.
Dziewonski, A.M., and Anderson, D.L. (1981) Preliminary reference Earth model. Physics of the Earth and Planetary Interiors, 25(4), 297–356.
Fei, Y., Ricolleau, A., Frank, M., Mibe, K., Shen, G., and Prakapenka, V. (2007) Toward an internally consistent pressure scale. Proceedings of the National Academy of Sciences, 104(22), 9182–9186.
Finger, W., and Ohashi, N.Y. (1976) The thermal expansion of diopside to 800 °C and a refinement of the crystal structure at 700 °C. American Mineralogist, 61, 303–310.
Finkelstein, G.J., Dera, P.K., Jahn, S., Oganov, A.R., Holl, C.M., Meng, Y., and Duffy, T.S. (2014) Phase transitions and equation of state of forsterite to 90 GPa from single-crystal X-ray diffraction and molecular modeling. American Mineralogist, 99(1), 35–43.
Frost, D.J. (2008) The upper mantle and transition zone. Elements, 4(3), 171–176.
Fukao, Y., and Obayashi, M. (2013) Subducted slabs stagnant above, penetrating through, and trapped below the 660 km discontinuity. Journal of Geophysical Research: Solid Earth, 118(11), 5920–5938.
Fukao, Y., Widiyantoro, S., and Obayashi, M. (2001) Stagnant slabs in the upper and lower mantle transition region. Reviews of Geophysics, 39(3), 291–323.
Ganguly, J., Freed, A.M., and Saxena, S.K. (2009) Density profiles of oceanic slabs and surrounding mantle: Integrated thermodynamic and thermal modeling, and implications for the fate of slabs at the 660km discontinuity. Physics of the Earth and Planetary Interiors, 172(3), 257–267.
Grand, S.P. (2002) Mantle shear–wave tomography and the fate of subducted slabs. Philosophical Transactions of the Royal Society of London A: Mathematical, Physical and Engineering Sciences, 360(1800), 2475–2491.
Green, D., and Ringwood, A. (1967) The stability fields of aluminous pyroxene peridotite and garnet peridotite and their relevance in upper mantle structure. Earth and Planetary Science Letters, 3, 151–160.
Hazen, R.M., and Finger, L.W. (1977) Compressibility and crystal structure of Angra dos Reis fassaite to 52 kbar. Carnegie Institution of Washington Year Book, 76, 512–515.
Hu, Y., Dera, P., and Zhuravlev, K. (2015) Single-crystal diffraction and Raman spectroscopy of hedenbergite up to 33 GPa. Physics and Chemistry of Minerals, 42, 595–608.
Ito, E., and Takahashi, E. (1989) Postspinel transformations in the system Mg_2SiO_4-Fe_2SiO_4 and some geophysical implications. Journal of Geophysical Research:

Solid Earth, 94(B8), 10637–10646.

Kantor, I., Prakapenka, V., Kantor, A., Dera, P., Kurnosov, A., Sinogeikin, S., Dubrovinskaia, N., and Dubrovinsky, L. (2012) BX90: A new diamond anvil cell design for X-ray diffraction and optical measurements. Review of Scientific Instruments, 83(12), 125102.

Kawakatsu, H., and Yoshioka, S. (2011) Metastable olivine wedge and deep dry cold slab beneath southwest Japan. Earth and Planetary Science Letters, 303(1), 1–10.

King, S.D., Frost, D.J., and Rubie, D.C. (2015) Why cold slabs stagnate in the transition zone. Geology, 43(3), 231–234.

Knight, K.S. (2010) Analytical expressions to determine the isothermal compressibility tensor and the isobaric thermal expansion tensor for monoclinic crystals: application to determine the direction of maximum compressibility in jadeite. Physics and Chemistry of Minerals, 37(8), 529–533.

Levien, L., and Prewitt, C.T. (1981) High-pressure structural study of diopside. American Mineralogist, 66, 315–323.

Li, C., van der Hilst, R.D., Engdahl, E.R., and Burdick, S. (2008) A new global model for P wave speed variations in Earth's mantle. Geochemistry, Geophysics, Geosystems, 9(5).

Liu, L.-G. (1976) The post-spinel phase of forsterite. Nature, 262, 770–772.

McCarthy, A.C., Downs, R.T., and Thompson, R.M. (2008a) Compressibility trends of the clinopyroxenes, and in-situ high-pressure single-crystal X-ray diffraction study of jadeite. American Mineralogist, 93(1), 198–209.

McCarthy, A.C., Downs, R.T., Thompson, R.M., and Redhammer, G.J. (2008b) In situ high-pressure single-crystal X-ray study of aegirine, $NaFe^{3+}Si_2O_6$, and the role of M1 size in clinopyroxene compressibility. American Mineralogist, 93, 1829–1837.

Nestola, F., Ballaran, T.B., Liebske, C., Bruno, M., and Tribaudino, M. (2006) High-pressure behaviour along the jadeite $NaAlSi_2O_6$-aegirine $NaFeSi_2O_6$ solid solution up to 10 GPa. Physics and Chemistry of Minerals, 33(6), 417–425.

Nishi, M., Kato, T., Kubo, T., and Kikegawa, T. (2008) Survival of pyropic garnet in subducting plates. Physics of the Earth and Planetary Interiors, 170(3), 274–280.

Nishi, M., Kubo, T., and Kato, T. (2009) Metastable transformations of eclogite to garnetite in subducting oceanic crust. Journal of Mineralogical and Petrological Sciences, 104(3), 192–198.

Nishi, M., Kubo, T., Ohfuji, H., Kato, T., Nishihara, Y., and Irifune, T. (2013) Slow Si–Al interdiffusion in garnet and stagnation of subducting slabs. Earth and Planetary Science Letters, 361, 44–49.

Nishihara, Y., Takahashi, E., Matsukage, K., and Kikegawa, T. (2003) Thermal equation of state of omphacite. American Mineralogist, 88, 80–86.

O'Har, M. (1961) Petrology of the Scourie dyke, Sutherland. Mineralogical Magazine, 32, 848–865.

Ohashi, Y. (1982) STRAIN, a program to calculate the strain tensor from two sets of unit-cell parameters. In R.M. Hazen and L.W. Finger, Eds., Comparative Crystal Chemistry, Wiley, New York, pp. 92–102.

Otten, M.T., and Buseck, P.R. (1987) TEM study of the transformation of augite to sodic pyroxene in eclogitized ferrogabbro. Contributions to Mineralogy and Petrology, 96(4), 529–538.

Plonka, A.M., Dera, P., Irmen, P., Rivers, M.L., Ehm, L., and Parise, J.B. (2012) β-diopside, a new ultrahigh-pressure polymorph of $CaMgSi_2O_6$ with six-coordinated silicon. Geophysical Research Letters, 39(24).

Posner, E.S., Dera, P., Downs, R.T., Lazarz, J.D., and Irmen, P. (2014) High-pressure single-crystal X-ray diffraction study of jadeite and kosmochlor. Physics and Chemistry of Minerals, 41(9), 695–707.

Richet, P., Mysen, B.O., and Ingrin, J. (1998) High-temperature X-ray diffraction and Raman spectroscopy of diopside and pseudowollastonite. Physics and Chemistry of Minerals, 25(6), 401–414.

Ringwood, A.E. (1982) Phase transformations and differentiation in subducted lithosphere: implications for mantle dynamics, basalt petrogenesis, and crustal evolution. The Journal of Geology, 611–643.

Rivers, M., Prakapenka, V.B., Kubo, A., Pullins, C., Holl, C.M., and Jacobsen, S.D. (2008) The COMPRES/GSECARS gas-loading system for diamond anvil cells at the Advanced Photon Source. High Pressure Research, 28(3), 273–292.

Robinson, K., Gibbs, G., and Ribbe, P. (1971) Quadratic elongation: a quantitative measure of distortion in coordination polyhedra. Science, 172, 567–570.

Rooney, T.O., Furman, T., Yirgu, G., and Ayalew, D. (2005) Structure of the Ethiopian lithosphere: Xenolith evidence in the Main Ethiopian Rift. Geochimica et Cosmochimica Acta, 69(15), 3889–3910.

Schlinger, C.M., and Veblen, D.R. (1989) Magnetism and transmission electron microscopy of Fe-Ti oxides and pyroxenes in a granulite from Lofoten, Norway. Journal

of Geophysical Research: Solid Earth, 94(B10), 14009–14026.

Schorn, S., and Diener, J.F. (2016) Details of the gabbro–to–eclogite transition determined from microtextures and calculated chemical potential relationships. Journal of Metamorphic Geology, doi:10.1111/jmg.12220.

Sheldrick, G.M. (2007) A short history of SHELX. Acta Crystallographica, A64(1), 112–122.

Shinmei, T., Tomioka, N., Fujino, K., Kuroda, K., and Irifune, T. (1999) In situ X-ray diffraction study of enstatite up to 12 GPa and 1473 K and equations of state. American Mineralogist, 84, 1588–1594.

Takeda, H., Yugami, K., Bogard, D., and Miyamoto, M. (1997) Plagioclase-augite-rich gabbro in the Caddo County IAB iron, and the missing basalts associated with iron meteorites. Lunar and Planetary Science Conference, 28, 409.

Thompson, R.M., and Downs, R.T. (2008) The crystal structure of diopside at pressure to 10 GPa. American Mineralogist, 93, 177–186.

Tracy, R., and Robinson, P. (1977) Zoned titanian augite in alkali olivine basalt from Tahiti and the nature of titanium substitutions in augite. American Mineralogist, 62, 634–645.

Tribaudino, M., and Mantovani, L. (2014) Thermal expansion in $C2/c$ pyroxenes: a review and new high-temperature structural data for a pyroxene of composition $(Na_{0.53}Ca_{0.47})(Al_{0.53}Fe_{0.47})Si_2O_6$ ($Jd_{53}Hd_{47}$). Mineralogical Magazine, 78(2), 311–324.

Tribaudino, M., Nestola, F., Bruno, M., Boffa Ballaran, T., and Liebske, C. (2008) Thermal expansion along the $NaAlSi_{(2)}O_{(6)}$-$NaFe^{(3+)}Si_{(2)}O_{(6)}$ and $NaAlSi_{(2)}O_{(6)}$-$CaFe^{(2+)}Si_{(2)}O_{(6)}$ solid solutions. Physics and Chemistry of Minerals, 35(5), 241–248.

Ullrich, A., Miletich, R., Balic-Zunic, T., Olsen, L., Nestola, F., Wildner, M., and Ohashi, H. (2010) (Na, Ca)(Ti^{3+}, Mg) Si_2O_6-clinopyroxenes at high pressure: influence of cation substitution on elastic behavior and phase transition. Physics and Chemistry of Minerals, 37(1), 25–43.

Van der Hilst, R., Widiyantoro, S., and Engdahl, E. (1997) Evidence for deep mantle circulation from global tomography. Nature, 386, 578–584.

Van Mierlo, W., Langenhorst, F., Frost, D., and Rubie, D. (2013) Stagnation of subducting slabs in the transition zone due to slow diffusion in majoritic garnet. Nature Geoscience, 6(5), 400–403.

Xu, J., Kuang, Y., Zhang, B., Liu, Y., Fan, D., Li, X., and Xie, H. (2016) Thermal equation of state of natural tourmaline at high pressure and temperature. Physics and Chemistry of Minerals, 43(5), 315–326.

Xu, J., Zhang, D., Fan, D., Downs, R.T., Hu, Y., and Dera, P. (2017) Isosymmetric pressure-induced bonding increase changes compression behavior of clinopyroxenes across jadeite-aegirine solid solution in subduction zones. Journal of Geophysical Research: Solid Earth, 122(1), 142–157.

Yang, H., and Prewitt, C.T. (2000) Chain and layer silicates at high temperatures and pressures. Reviews in Mineralogy and Geochemistry, 41(1), 211–255.

Zhang, L., Ahsbahs, H., Hafner, S.S., and Kutoglu, A. (1997) Single-crystal compression and crystal structure of clinopyroxene up to 10 GPa. American Mineralogist, 82(3), 245–258.

Zhang, L., Stanek, J., Hafner, S., Ahsbahs, H., Grünsteudel, H., and Metge, J. (1999) ^{57}Fe nuclear forward scattering of synchrotron radiation in hedenbergite $CaFeSi_2O_6$ at hydrostatic pressures up to 68 GPa. American Mineralogist, 84(3), 447–453.

Zhang, J.S., Dera, P., and Bass, J.D. (2012) A new high-pressure phase transition in natural Fe-bearing orthoenstatite. American Mineralogist, 97(7), 1070–1074.

Zhang, D., Hu, Y., and Dera, P.K. (2016) Compressional behavior of omphacite to 47 GPa. Physics and Chemistry of Minerals, 43(10), 707–715.

Zhang, D., Dera, P.K., Eng, P.J., Stubbs, J.E., Zhang, J.S., Prakapenka, V.B., and Rivers, M.L. (2017) High pressure single crystal diffraction at PX^2. Journal of Visualized Experiments, 119, e54660, doi:10.3791/54660.

Zhao, Y., Dreele, R.V., Zhang, J., and Weidner, D. (1998) Thermoelastic equation of state of monoclinic pyroxene: $CaMgSi_2O_6$ diopside. The Review of High Pressure Science and Technology, 7, 25–27.

Zhao, Y., Von Dreele, R.B., Shankland, T.J., Weidner, D.J., Zhang, J., Wang, Y., and Gasparik, T. (1997) Thermoelastic equation of state of jadeite $NaAlSi_2O_6$: An energy-dispersive Reitveld refinement study of low symmetry and multiple phases diffraction. Geophysical Research Letters, 24(1), 5–8.